JOURNAL OF MATERIALS SCIENCE 28 (1993) 1879–1884

Dispersive behaviour of humid anisotropic media

A. K. JONSCHER, B. N. AYUB*
Physics Department, Royal Holloway College, University of London, Egham, Surrey TW20 0EX, UK

The results of dielectric measurements on a humid system consisting of filter papers which show strongly anisotropic properties in the planes and normal to the planes of the sheets, are reported. Configurations were used in which the flow of current is, respectively, normal to and in the planes and these show distinctively different behaviour. Transport in the planes provides some of the best examples of LFD ever seen by us, extending over up to eight decades of frequency; transport across the planes is influenced by less dispersive behaviour which is ascribed to the fibre–fibre contacts.

1. Introduction – low-frequency dispersion

The availability in recent years of frequency response analysers (FRAs) enabling dielectric measurements to be made down to very low frequencies in the milli-Hertz range [1], and the corresponding time-domain instrumentation have opened up the studies of low-frequency phenomena which show completely unexpected behaviour compared with typical behaviour at higher frequencies. In particular, it turns out that the dielectric response in the frequency domain (FD) and in the time domain (TD) of carrier-dominated systems, as distinct from dipolar systems, reveals features known as low-frequency dispersion (LFD) [2] in which the real and imaginary components of the complex dielectric susceptibility $\tilde{\chi}(\omega) = \tilde{\varepsilon}(\omega) - \varepsilon_\infty$ or of the corresponding capacitance equivalent $\tilde{X}(\omega) = K\tilde{\chi}(\omega) = \tilde{C}(\omega) - C_\infty$ follow two "universal" fractional power laws [3] of the form

$$\tilde{X}(\omega) = B_n(i\omega)^{n-1} \quad (1)$$

where B_n is a constant of dimensions $F\,S^{n-1} = S\,S^n$, $\tilde{\varepsilon}(\omega)$ is the complex dielectric permittivity, $\tilde{C}(\omega) = C'(\omega) - iC''(\omega)$ is the complex capacitance, ε_∞ is the limiting high-frequency value of the permittivity and C_∞ is the corresponding value of the capacitance, while K is a geometrical factor. At low frequencies the exponent n_2 is close to zero, while at high frequencies it is nearer to unity as would be the case of a low-loss capacitor. This is shown schematically in Fig. 1a.

The implication of Equation 1 is the ratio of the imaginary to the real components of $\tilde{X}$ is independent of frequency

$$X''(\omega)/X'(\omega) = \cot(n\pi/2) = \text{constant independent of frequency} \quad (2)$$

With small values of $n \approx 0.05$–0.1, Equation 2 yields a ratio of approximately 13 to 6, implying a very lossy universal capacitor, in complete contrast with the usual low-loss capacitors for which $n \approx 1$. Another very important departure from conventional dielectric behaviour is the presence of strong dispersion in the *real part* $X'(\omega)$, which in the limit of direct current (d.c.) conduction should remain strictly independent of frequency at sufficiently low frequencies, while $X''(\omega)$ should be strictly proportional to $1/\omega$. The conclusion is, therefore, that LFD entails a considerable storage of charge in the system.

Fig. 1b shows the corresponding TD charging, i_c, and discharging, i_d, currents which are the Fourier transforms of Equation 2

$$i_c(t) - i_0 = i_d(t) \propto t^{-n} \quad (3)$$

With small values of n these currents are very slowly varying with time and the fundamental difference with the d.c. behaviour is the finite discharging current. The d.c. current, i_0, is generally finite even in the presence of LFD.

The corresponding complex admittance is given by the following expressions

$$\tilde{Y}(\omega) = i\omega\tilde{C}(\omega) = B_n(i\omega)^n = A/d\tilde{\sigma}(\omega) \quad (4)$$

where we have introduced the frequency-dependent specific complex conductance

$$\tilde{\sigma}(\omega) = \sigma'(\omega) + i\sigma''(\omega) = i\omega\tilde{\varepsilon}(\omega) \quad (5)$$

which is related to the complex permittivity, $\tilde{\varepsilon}(\omega)$, and which represents a material property. A/d is a geometrical factor, A being the area of the electrodes and d

* Permanent address: Physics department, University of Karachi, Karachi 75270, Pakistan

0022–2461

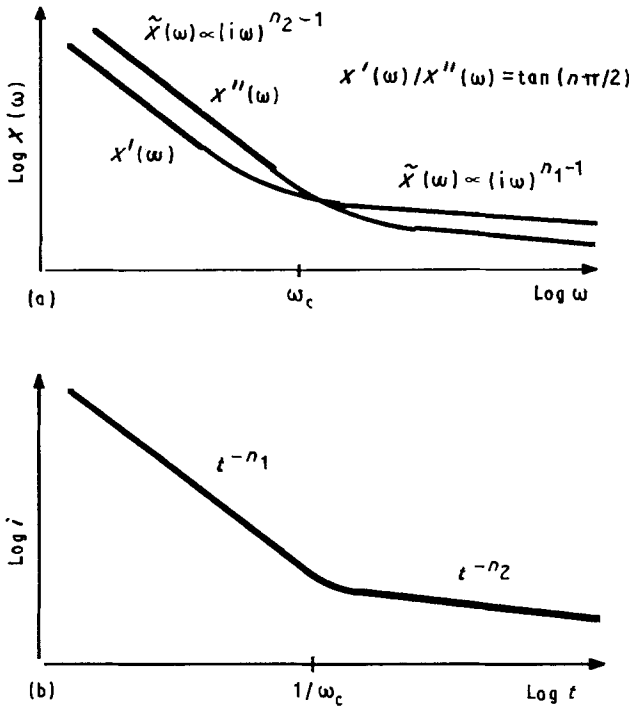

Figure 1 (a) A schematic presentation of the frequency-domain behaviour of a system showing LFD behaviour with the characteristic parallellism in the logarithmic plots of the real and imaginary components of the complex susceptance, $X'(\omega)$ and $X''(\omega)$, respectively. The high-frequency region corresponds to the normal low-loss behaviour of dielectrics, the low-frequency dispersive region is the LFD phenomenon. (b) The corresponding time-domain behaviour, with the long-time almost constant current corresponding to the low-frequency dispersive part of (a).

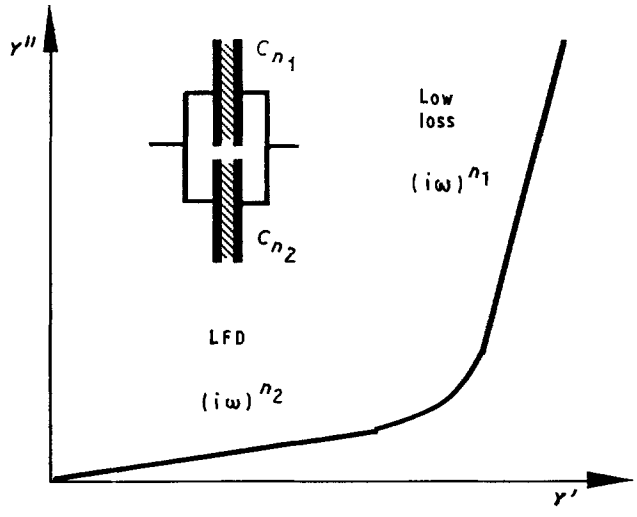

Figure 2 Schematic appearance of the complex admittance plot of a dielectric system characterized by the frequency dependence of the capacitance shown in Fig. 1a. The low-loss high-frequency branch is defined by an exponent, n_1, close to unity, the low-frequency highly lossy LFD branch has the exponent, n_2, close to zero. The behaviour is well represented by the parallel combination of two capacitors, C_{n_1} and C_{n_2}.

the distance between them. We note that $\sigma'(\omega)$ is the ordinary frequency-dependent conductivity. Equation 5 enables us to relate the admittances to the material properties regardless of the geometrical factors. In the perpendicular samples $d = Nw_{FP}$, where $w_{FP} = 0.16$ mm is the thickness of an individual filter paper and N is their number in the stack; in the parallel samples $A = Nw_{FP}l$ and $d = s$, where l and s are defined in Fig. 3 below.

The complex plane plot of $\tilde{Y}$ is shown in Fig. 2, and it has a steeply rising high-frequency branch corresponding to a low-loss capacitor, $\tilde{C}_{n_1}$, and a nearly horizontal low-frequency branch corresponding to our LFD capacitor, $\tilde{C}_{n_2}$, which may be considered to be in parallel with the former.

If the capacitors $\tilde{C}_{n_1}$ and $\tilde{C}_{n_2}$ are present in their "pure universal" form without any series resistance elements, their characteristics are straight lines with the appropriate ratio spacing in the logω plots and straight lines in the $\tilde{Y}$ plots. Any series elements would manifest themselves in a curvature of the $\tilde{Y}$ plots and in deviations from the simple LFD behaviour in the log$C$–logω plots.

2. LFD in anisotropic media

Our understanding of the physico-chemical nature of LFD is not adequate, even though a significant amount of experimental material is available [2]. It is significant that many of the well-documented examples of LFD relate to essentially two-dimensional flow, for example in zeolites where it takes place in the interiors of interconnected molecular cavities [4, 5], on mica and on glass [9].

In order to advance the understanding of the LFD processes we have undertaken a detailed study of the FD and TD response of humid filter papers which represent essentially highly pure fibrous cellulose with the predominant orientation of the fibres being in the plane of the paper, although a finite measure of "normal" orientation is also present. The particular aim of this investigation was to compare the behaviour along and at right angles to the fibres in the filter paper. Our samples consisted of stacks of filter papers of variable number, N, of papers between 1 and 80 sheets, sandwiched between massive end electrodes, pressed together by controlled force and placed in a desiccator with controlled relative humidity (RH) between virtually zero (silica gel) and 97%.

The advantage of these filter papers lies in the ability to insert potential electrodes between them and to study the distribution of this potential along the stack to assess the role of the electrodes. Details of the experimental arrangements and the general description of the results will be given in a separate publication, the present paper is concerned with the narrower aspect of the results in which the flow of current is, respectively, normal and parallel to the prevailing orientation of the fibres.

The samples were of two basic types, referred to as normal (FP $\perp$) and parallel (FP $\parallel$) with respect to the plane of the paper, i.e. with respect to the fibres, shown schematically in Fig. 3. The normal samples were held together by an axial compression screw under controlled pressure, the parallel samples were held in an insulating yoke. All samples were kept in the desiccator under controlled humidity for 2 weeks to achieve equilibrium with the atmosphere. The perpendicular samples had an area $A = 2.37 \times 10^{-3}$ m^2, the 10FP $\parallel$ and 40 FP $\parallel$ samples had $s = 10$ mm and

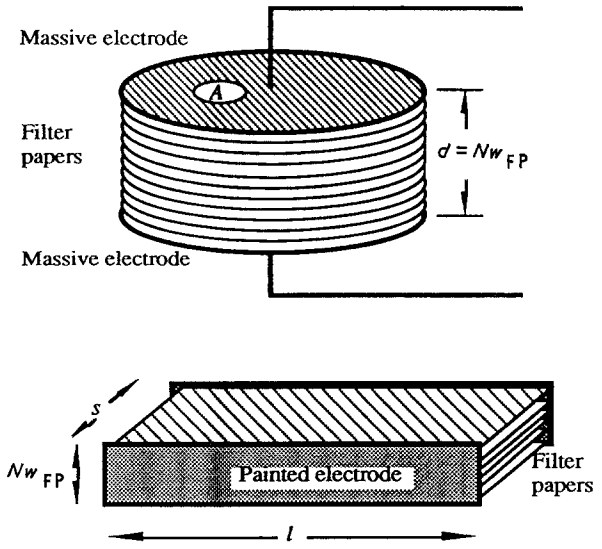

Figure 3 The two types of sample used in the present investigation. (a) The "perpendicular" sample in which the current flow is normal to the plane of the paper and to the preferred direction of the fibres; (b) the "parallel" sample in which the current flow direction is parallel to the plane of the fibres. In (a) there are massive electrodes of metals or of graphite of area A and the sample of thickness w is held together by normal force. In (b) the electrodes of area $w \times l$ are painted at the ends of strips of filter paper of length s held together by an insulating yoke. The number of filter papers in the perpendicular configuration is 1, 10 or 80, while in (b) it is 10 or 40. In the parallel configuration one single sheet was also measured, in which the electrodes were painted on one of its surfaces.

$l = 55$ mm. The electrode area of these samples was $A = Nw_{FP}l$. The single filter paper sample 1, FP ||, had $s = 8$ mm and $l = 40$ mm and its electrodes were painted on one surface of the paper, not on the edge, which would not have been practical.

3. Results

Fig. 4 shows the experimental data $C'(\omega)$ and $C''(\omega)$ for three parallel samples of 1, 10 and 40 filter papers (FP ||). There is, in this case, no need to subtract C_∞ because the effect of this would be negligible. The overall impression is that the logarithmic plots follow nearly straight lines with a nearly constant ratio $X''(\omega)/X'(\omega) \approx 5$–10, corresponding to a low-frequency exponent $n_2 \approx 0.10$–0.12. The factors B_n derived from these results at $\omega = 1$ are as given below, together with the corresponding values of $\sigma_\parallel = |\tilde{\sigma}|$ from Equation 4:

$B_n \approx 7.3 \times 10^{-7}\,\mathrm{F\,s^{-0.98}}$, $\sigma_\parallel \approx 9.2 \times 10^{-4}\,\mathrm{S\,m^{-1}}$, for 1 FP ||

$B_n \approx 1.85 \times 10^{-6}\,\mathrm{F\,s^{-0.9}}$, $\sigma_\parallel \approx 2.1 \times 10^{-4}\,\mathrm{S\,m^{-1}}$, for 10 FP ||

and $B_n \approx 8.8 \times 10^{-6}\,\mathrm{F\,s^{-0.9}}$, $\sigma_\parallel \approx 2.5 \times 10^{-4}\,\mathrm{S\,m^{-1}}$, for 40 FP ||

which scales correctly for 10 and 40 FP, while the agreement is less good for 1 FP, even allowing for the slightly different geometry.

The fact that the logarithmic plots of $C'(\omega)$ and $C''(\omega)$ are approximately, but not exactly, straight lines points to slight perturbations arising from additional

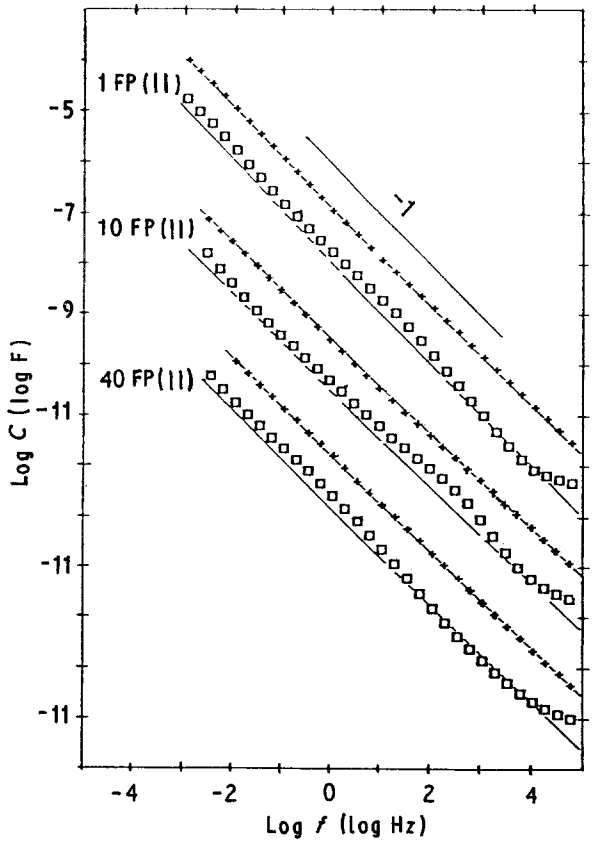

Figure 4 The frequency dependence of the capacitance of three parallel samples of 1, 10 and 40 filter papers, at 97% RH, showing an almost ideal LFD over more than seven decades of frequency. The three sets of data are displaced veritcally for clarity by three decades and the plots of $C'(\omega)$ and $C''(\omega)$ for 40 and 10 FP are in the expected ratio of approximately 4:1, allowing the slight deviations from straight lines, while the 1FP result is slightly out, but its geometry is rather less well defined.

processes apart from the principal LFD process. To establish more clearly the nature of these, we calculate the complex admittance which for the 40 FP || sample is shown in Fig. 5. There is a rising high-frequency "spur" which is clearly due to some relatively low-loss capacitance, $\tilde{C}_{n_1}(\omega)$, visible as the flattening of $C'(\omega)$ in Fig. 4 which may be subtracted, leaving a rather shallow arc completed by the circular points, suggesting the presence of some additional element in series with the LFD but which does not admit further detailed analysis.

The most significant conclusion from these results is the prevalence of a very clearly defined LFD spanning seven decades of frequency, with very little interference from other processes. This trend is indicated in Fig. 5 as the line of slope $n = 0.05$ which joins the origin to the tangent to the high-frequency spur.

We now turn to the direction of current flow normal to the planes of the filter papers and to the prevailing direction of the fibres. Fig. 6 shows the logarithmic plots of $C'(\omega)$ and $C''(\omega)$ for samples 10 FP$\perp$ and 80 FP$\perp$ with stainless steel electrodes at 97% RH and at 1 and 9 V r.m.s. amplitude. It is evident that the behaviour of these perpendicular samples is fundamentally different from that of the parallel samples shown in Fig. 4, in that the near-ideal LFD response of the latter is complicated by the strong influence of parallel and series components which have to be

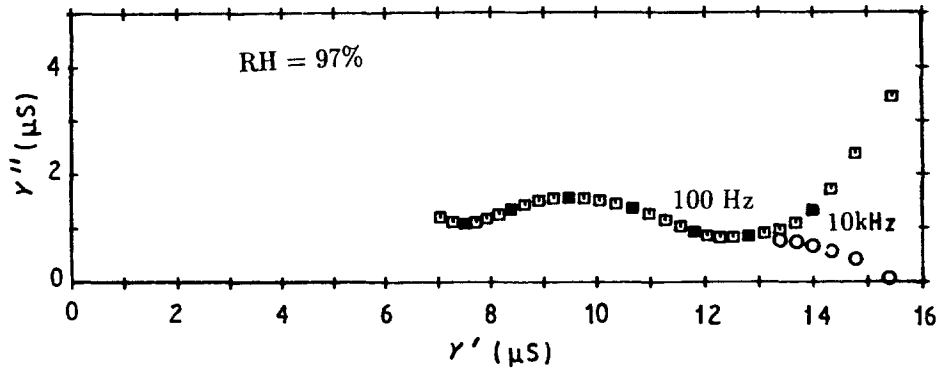

Figure 5 The complex admittance diagram of the 40 FP || sample at 97% RH showing a steep rise at high frequencies corresponding to the flattening $C'(\omega)$ and a broad flat arc stretching over five decades of frequency being responsible for slight waviness of the $\tilde{C}(\omega)$ plots. The $C'(\omega)$ plot is extended at high frequencies by subtracting a value of C_∞. The behaviour below 1 kHz may be considered as a superposition of the broad arc on the LFD.

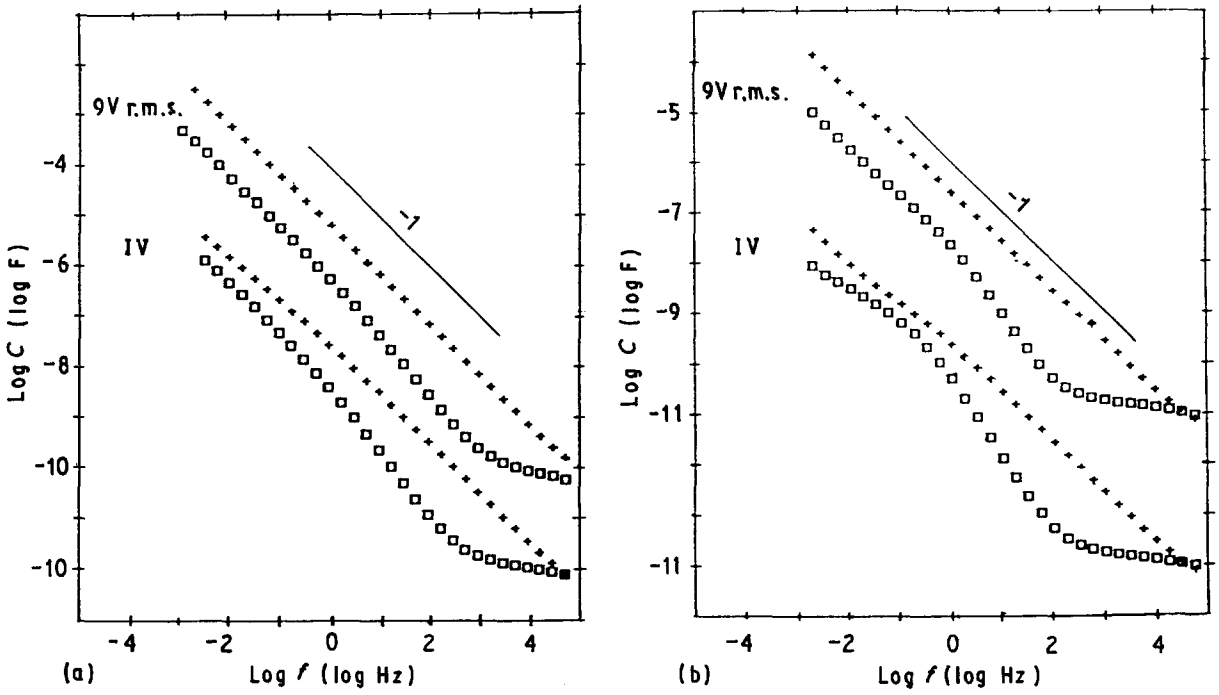

Figure 6 The frequency dependence of the capacitance of two normal samples of 10 and 80 FP⊥ at 97% RH, with stainless steel electrodes and with two signal amplitudes of 1 and 9 V r.m.s. These show LFD strongly perturbed by extraneous processes and also some non-linearity of response. The logarithmic slopes of -1 are indicated to reveal the correct behaviour at lower frequencies where this LFD process is seen in its pure form.

resolved by admittance transformation. The high-frequency capacitance of the two samples scales correctly in the ratio of 80:10 and so does, to a lesser extent, their loss. The effect of increasing signal amplitude is stronger in the thicker sample and it tends to make the LFD behaviour more pronounced. Thus the LFD behaviour is clearer at larger amplitudes and in the thinner sample.

Measurements on a similar stack of filter papers between graphite electrodes have shown very similar results. Evaluating the numerical parameters from the low-frequency ($\omega = 1$) end of the spectrum we obtain approximately

$B_n \approx 4.3 \times 10^{-4}\,\mathrm{F\,s^{-0.7}}$, $\sigma_\perp \approx 2.9 \times 10^{-5}\,\mathrm{S\,m^{-1}}$, for 1 FP⊥

$B_n \approx 1.5 \times 10^{-5}\,\mathrm{F\,s^{-0.9}}$, $\sigma_\perp \approx 1.0 \times 10^{-5}\,\mathrm{S\,m^{-1}}$, for 10 FP ⊥

and $B_n \approx 1.2 \times 10^{-6}\,\mathrm{F\,s^{-0.76}}$,

$\sigma_\perp \approx 0.64 \times 10^{-5}\,\mathrm{S\,m^{-1}}$, for 80 FP ⊥

We note the difference between these values and those for FP ||, the former being of the order of $\approx 2 \times 10^{-4}$, except for 1 FP ||, compared to $\approx 10^{-5}$ for FP ⊥, suggesting an approximately 20 times higher conductivity along the fibres than across them. This is not surprising, given that $\sigma_\perp$ are dominated by transitions across fibre–fibre contacts, while $\sigma_\parallel$ are determined predominantly by transport along the individual fibres.

Now if the end electrodes were to contribute a significant series effect, this would be more pronounced in the thinner sample, but it is significant that there does not appear to be any evidence for a series element in the impedance plots. This is confirmed by direct potential probing (under steady state

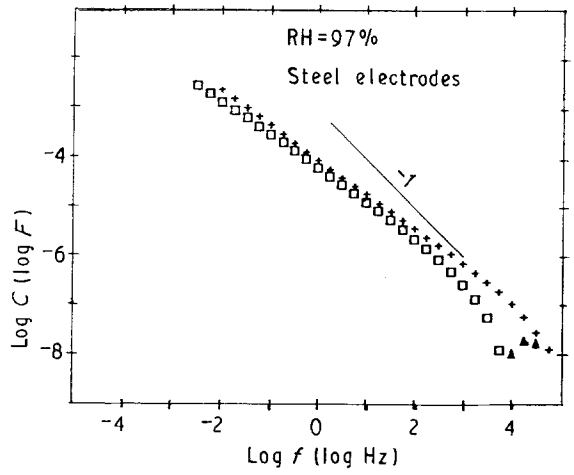

Figure 7 The complex capacitance of 1 FP⊥ at 97% RH between stainless steel electrodes showing a region of negative capacitance at high frequencies masking the low-loss capacitance region present in Fig. 6. The almost perfect power law at low frequencies corresponds to $n = 0.37$.

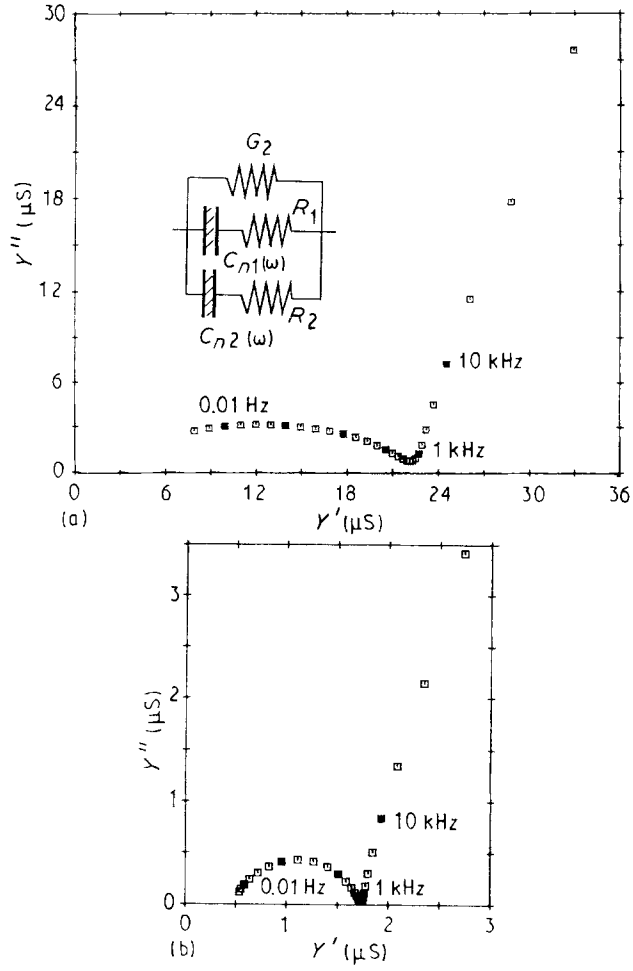

Figure 8 The admittance plots of the (a) 10 and (b) 80 FP⊥ samples with stainless steel electrodes, both at 1 V r.m.s., shown in Fig. 5. Both reveal a nearly straight-line high-frequency "spur" corresponding to a relatively low-loss "universal" capacitor, $\tilde{C}_{n_1}(\omega)$, and a low-frequency arc corresponding to a series combination of a strongly dispersive capacitor, $\tilde{C}_{n_2}(\omega)$, and a resistor, R. In the case of 80 FP⊥ the arc is less strongly inclined than for 10 FP⊥, in conformity with the much lower slope of the $\tilde{C}_{n_2}(\omega)$ plot. There is also clear evidence of a parallel conductance. The inset shows the equivalent circuit of the samples.

conditions) along the samples, which reveals only a slight drop at either end electrode, with most of the potential being distributed in the "bulk" of the samples.

The corresponding admittance plots are shown in Fig. 8 in which there is a clear division into two branches, a high-frequency nearly straight line "spur" corresponding to a not very lossy capacitor, $\tilde{C}_{n_1}(\omega)$, with $n_1 \approx 0.8$, and a low frequency arc which is rather shallow for the 10 FP sample and more nearly a semicircle for the 80 FP sample, the latter showing a clear intercept, G_2, on the real axis. The implication is that the low-frequency behaviour is represented by a lossy capacitor, $\tilde{C}_{n_2}$, with a series resistance. The difference in the inclination of the circular arcs of the 80 FP and 10 FP samples reflects the fact that the low-frequency branch of the 80 FP sample in Fig. 5 shows a less steep slope than that for the 10 FP sample.

An extreme example of the transverse configuration is shown in Fig. 7 giving the results for a single sheet of filter paper, 1 FP⊥, between stainless steel electrodes. There is no evidence of any flattening of $C'(\omega)$ towards high frequencies; instead a region of negative capacitance appears there. The response is otherwise almost pure LFD with a value of $n \approx 0.37$ but the admittance plot in Fig. 9 reveals the presence of a single skewed arc which might be interpreted as a series combination of an LFD element and a resistance.

4. Discussion

The principal conclusion from the data presented above is that the anisotropic medium represented by the stack of filter papers shows low frequency dispersion (LFD) in both directions, but transport in the plane of the fibres shows a mean volumetric conductivity, $\sigma_{\parallel}$, which is some 20 times higher than the conductivity, $\sigma_{\perp}$, across the planes of the filter papers. Furthermore, transport in the planes is characterized by a much simpler form of response, giving almost pure LFD stretching over nearly eight decades of frequency with very few perturbing effects due to contacts or other complications.

By comparison, transverse transport consists of two parallel processes, one of which is represented by a relatively weakly dispersive universal capacitance, $\tilde{C}_{n_1}(\omega) \propto (i\omega)^{n-1}$, with the exponent $n \approx 0.8$, i.e. a not very lossy capacitor. The magnitude of this capacitor scales well with the geometrical dimensions of the stack of filter papers and we have to conclude that it represents the dielectric response of the stack of filter papers which do not make good contact with one another and the loss arises from the transverse polarization of the individual fibres.

The other component dominating low frequencies is represented by a complex arc in the admittance plane, which may be considered to correspond to a series connection of a strongly dispersive element and a capacitive element, which may be envisaged as resulting from a percolative transport across the planes of the fibres which is strongly influenced by fibre–fibre contacts and also entails the inevitable component of transport along the fibres, as shown schematically in

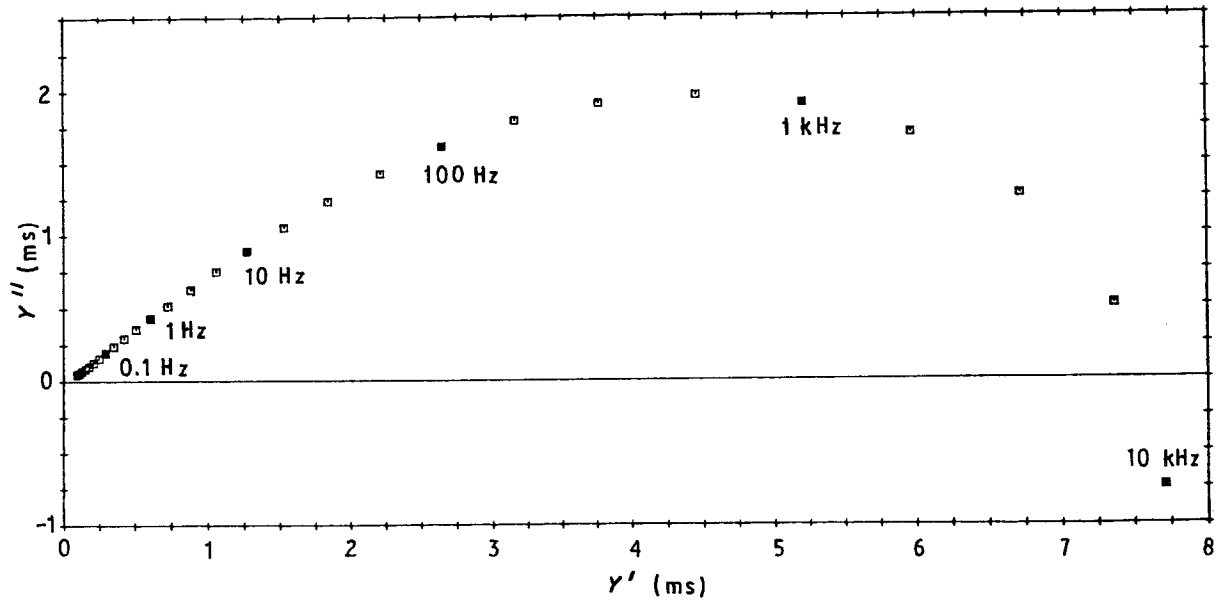

Figure 9 The complex admittance plot of the 1 FP ⊥ sample at 97% RH the capacitance of which is shown in Fig. 7. There is, in this case, no trace of the high-frequency spur, only a strongly inclined arc going through the origin with the low-frequency tangent giving a power law with $n = 0.37$ which corresponds well to the low-frequency slope of the log$C$–logω plots in Fig. 7.

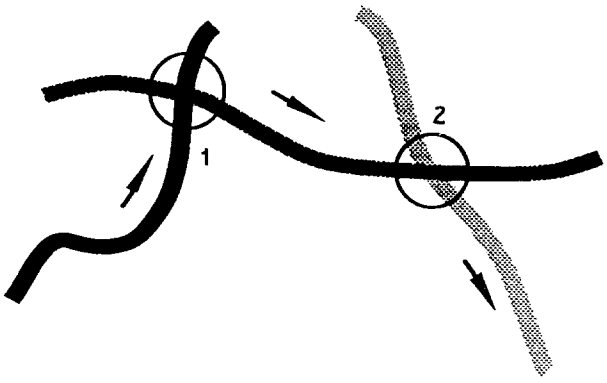

Figure 10 A schematic representation of transport across layers of fibres indicated here by progressively lighter shading for lower lying layers. The current in the top fibre indicated by the arrow on the left has to cross junction 1 between the two fibres in consecutive layers, to continue along the middle layer fibre until it reaches junction 2, when it passes to the lowest layer. This combination of strongly dispersive "easy" transport along filaments and relatively more difficult but less dispersive transport across fibre–fibre junctions results in the weakly dispersive nature of the capacitor $\tilde{C}_{n_1}(\omega)$.

Fig. 10. It is this component which is responsible for the lower value of $\sigma_\perp$ compared with $\sigma_\parallel$.

By and large, the response scales with the dimensions of the thicker samples, less well in the limit of single sheet samples. There is relatively little difference between the behaviour of samples with graphite and stainless steel electrodes.

There is no evidence in our experimental data of dominant effects of metallic electrodes; a slight effect is shown to be present by a finite potential drop at the electrodes, with most of the potential being dropped across the volume of the stack – this will be described in more detail in a separate publication. A direct confirmation of this conclusion is found in the fact that thinner transverse samples show, if anything, smaller effects that could be attributed to contacts, than do thick stacks.

Very thin samples in the transverse direction show relatively simple LFD behaviour with hardly any parallel effects, but their complex impedance reveals a series combination of a lossy capacitor and a resistor.

More detailed results, including time-domain charging and discharging currents, the effects of different electrode materials and of relative humidities intermediate between 0% and 97%, will be published separately.

Acknowledgements

One of us (BNA) acknowledges the tenure of a grant from the Overseas Development Administration administered by the British Council and also a study leave from the University of Karachi.

References

1. J. PUGH, "Dielectric Measurements Using Frequency Response Analysers", DMMA 1984, IEE Publication 239 (1984) pp. 247–50.
2. A. K. JONSCHER, *J. Mater. Sci.* **26** (1991) 1618.
3. *Idem*, "Dielectric Relaxation in Solids" (Chelsea Dielectrics Press, London, 1983).
4. A. R. HAIDAR and A. K. JONSCHER, *J. Chem. Soc. Faraday Trans. 1* **82** (1986) 3535.
5. A. K. JONSCHER and A. R. HAIDAR, *ibid.* **82** (1986) 3553.
6. M. A. CHAUDHRY and A. K. JONSCHER, *J. Mater. Sci.* **20** (1985) 3581.
7. A. K. JONSCHER and T. RAMDEEN, *IEEE Trans.* **EI-22** (1987) 35.
8. N. BANO and A. K. JONSCHER, *J. Mater. Sci.* **27** (1992) 1672.
9. E. F. OWEDE and A. K. JONSCHER. *J. Electrochem. Soc.* **135** (1988) 1757.

Received 12 February
and accepted 30 March 1992